IOP Conf. Series: Journal of Physics: Conf. Series **876** (2017) 012011 doi:10.1088/1742-6596/876/1/012011

Effect of breakup and resonance states of ^{6}Li on fusion

A. Gómez Camacho

Departamento de Aceleradores. Instituto Nacional de Investigaciones Nucleares, Apartado Postal 18-1027, C.P. 11801, México, D.F.

Abstract. CDCC calculations of total fusion cross sections are presented for reactions of the weakly bound ^{6}Li with targets ^{144}Sm and ^{154}Sm at energies around the Coulomb barrier. Couplings to the low-lying excited states 2^+, 3^- of ^{144}Sm and 2^+, 4^+ of ^{154}Sm are included in the calculations. In the cluster structure frame of ^{6}Li$\rightarrow \alpha + d$, short range absorption potentials are considered for the interactions between α- and d- with the target to account for fusion. The effect of the excited states of the target on total fusion is investigated, as well as, that from couplings of resonance states of ^{6}Li, namely, $l = 2, J^\pi = 3^+, 2^+, 1^+$. The latter effect is calculated by two different approaches, (a) by considering only resonance states couplings and (b) by omitting these states from the full discretized energy space. Among other things, it is found that resonance and non-resonance continuum couplings give rise to small and similar fusion suppression at the higher energies.

1. Introduction

Lately, reaction mechanisms involving weakly bound nuclei, both stable and radioactive, have been a subject of strong research [1, 2, 3, 4, 5]. Among the most interesting and studied subjects is the effect of breakup of the weakly bound projectile on elastic scattering and fusion reaction processes. The characteristic low binding energy associated to this type of projectiles affects reaction mechanisms mainly in two ways. Namely, the static effect due to the large diffusivity of the projectile matter density. This stretched density lowers the Coulomb barrier and hence enhance fusion. On the other side, the high projectile breakup probability produces strong repulsive couplings that affect elastic and fusion mechanisms. The repulsive polarization potentials so produced, are most important at energies around the barrier and thus, cause fusion suppression.

Other features of reactions with weakly bound nuclei that have been a topic of experimental and theoretical research are the different fusion mechanisms that take place, that is, complete and incomplete fusion. Complete fusion (CF) can be direct complete fusion (DCF) which is a process similar to fusion between strongly bound nuclei, that is, fusion that occurs without a previous excitation of breakup channels. Also, the Sequential complete fusion (SCF) that consists of fusion of all the projectile fragments after a previous breakup. From an experimental point of view, it is very difficult to distinguish the evaporation products from a compound nucleus produced by DCF or SCF, for that reason, only the sum of CF and SCF can be measured. On the other hand, another reaction mechanism is the incomplete fusion (ICF), which is the partial absorption of some fragments while others fly away to the continuum. Total fusion TF,

commonly the quantity measured, is the sum of the complete and incomplete fusion. Recently the separate experimental determination of complete and incomplete fusion has been achieved for some reactions with light weakly bound projectiles on medium mass and heavy targets. This has been possible since, contrary to the case of light targets, the compound nucleus decays by the emission of uncharged particles [6, 7, 8]. Another process with weakly bound projectiles is the elastic breakup (EB), in which none of the fragments after breakup is absorbed by the target. It is now well known that in reactions with weakly bound nuclei, couplings from the elastic channel to continuum breakup states, as well as, continuum-continuum couplings have a profound effect on elastic and fusion mechanisms. To study these effects, a complete theoretical description should include all of the aforementioned reaction processes in a single calculation. Presently, the most powerful theoretical tool to do this type of calculations is the Continuum Discretized Coupled-Channel (CDCC) model[9, 10, 11]. This approach has been used to a large range of weakly bound nuclear systems, for instance; the $2n$-halo ^{6}He projectile on ^{59}Co and ^{208}Pb [12, 13], ^{6}Li with targets ^{28}Si, ^{59}Co, ^{58}Ni, ^{144}Sm and ^{208}Pb [9, 12, 14, 15, 16, 17, 18, 19]. Also, ^{7}Li with ^{28}Si [20, 21] and ^{144}Sm [22], the n-halo ^{11}Be with ^{208}Pb [23] and the p-halo ^{8}B with ^{58}Ni [16, 24], ^{12}C [25] and ^{208}Pb [26].

Due to the experimental difficulty to perform separate measurements of complete and incomplete fusion cross sections, most of these studies have considered the effect of breakup couplings on either elastic scattering or total fusion processes. However, recently measurements of CF and ICF have been reported for some weakly bound nuclei with spherical and deformed medium mass targets. For instance, ^{6}Li with targets ^{90}Zr [27], ^{144}Sm and ^{152}Sm [28, 29] and also, the projectile ^{9}Be with ^{181}Ta [30], ^{169}Tm and ^{187}Re [31]. Similarly, theoretical studies that account for the effect of breakup on complete fusion have been performed for a number of systems, see Refs. [32, 33]. In a recent article [34], measurements of complete and incomplete fusion cross sections for the weakly bound ^{6}Li projectile with the highly deformed target ^{154}Sm at energies above the barrier are presented. Also, in this article, coupled-channel calculations are used to study the effect on complete fusion due to couplings to inelastic excited states of ^{154}Sm. As expected, it was found that, this effect is increasingly important as the energy decreases towards the barrier. A comparison of these results with those for the spherical ^{144}Sm with the same projectile ^{6}Li was also discussed. In the present work, CDCC calculations for these systems show that the effect of couplings to excited states of the spherical isotope ^{144}Sm and the largely deformed ^{154}Sm produce an increasing total fusion enhancement as the collision energy decreases below the barrier. As, it will be shown, this effect is more evident for ^{154}Sm than for ^{144}Sm. So, couplings to inelastic excited states of the target produce attractive polarization potentials that lower the fusion barrier. The strengths of these potentials increase for rotational deformed states. It is interesting to point out that total fusion σ_{TF} being composed by CF and ICF, is in principle unaffected by breakup Refs.[1, 35, 36, 37]. However, some enhancement has been found at energies around and below the barrier for the projectiles ^{6}Li, ^{7}Li with targets ^{59}Co and ^{209}Bi [38]. In the calculations, we assume the cluster structure of ^{6}Li$\rightarrow \alpha + d$ ($E_{thres} = -1.47$ MeV). Now, since the masses of the fragments α and d are not so different, their center of mass is not strongly directed towards one of them. Therefore, total fusion can not be calculated by the absorption of their center of mass as in other weakly bound nuclei. For instance, as in the case of the projectile $^{11}Be \rightarrow ^{10}Be + n$ for which, the absorption of the center of mass of ^{11}Be ensures the capture of the charged core ^{10}Be[39]. To calculate total fusion, the approach given in Ref. [38] is used. That is, two short-range imaginary potentials, inside the $l = 0$ nominal Coulomb barrier, are used to account for absorption of both or any of the fragments α and d by the target. So, complete and incomplete fusion are implicitly accounted for in this way. These imaginary potentials depend on the relative distance between the fragments and the target. In a different calculation, the effect of continuum resonance state couplings of the weakly bound nucleus ^{6}Li on total fusion is also studied. We follow a similar technique as in Refs. [40, 41], where the

effect on elastic scattering from couplings to resonance continuum states of ^{6}Li was determined for reactions with targets ^{28}Si, ^{58}Ni and ^{144}Sm. It was found that resonant states have some important effect on elastic scattering at the lowest collision energies and for the lightest targets. As a matter of fact, resonant state couplings produce a net repulsive polarization potential that reduces incoming flux absorption. Following a similar technique, the effect of continuum resonance states $l = 2$, $j^\pi = 3^+, 2^+$, 1^+ of ^{6}Li on total fusion is studied in this work. That is, two approaches are used: i) Omit resonant states from the full discretized breakup space and ii) Consider only the resonance states in the CDCC calculation of fusion, that is, all non-resonance states are omitted.

In section II, a brief description of the CDCC model is given. Section III is dedicated to give a detailed description of the construction of the CDCC discretized energy space for resonance and non-resonance states. A full description and calculations of total fusion cross sections are also given. The results of the effects on fusion from inelastic excited states of the target, as well as, from resonance and non-resonance continuum breakup couplings of the projectile are given as well. Finally, a summary and conclusions are presented in section IV.

2. Brief CDCC description

A complete description of the CDCC method is given in Refs.[9, 10, 11]. Here, only the basic equations that are required to perform our calculations are presented. We consider the two-body cluster structure of ^{6}Li (α-d) with ground state energy $E_{thres} = -1.47$ MeV. The model space for the ground and continuum states of ^{6}Li is that given in Ref. [38]. The wave function for breakup continuum states of ^{6}Li reads as,

$$\psi^P_{lj}(\mathbf{r}, k) = \{Y_{lm_l}(\hat{\mathbf{r}}) \otimes \chi_{I\mu s\sigma}\}_{lj} \frac{\varphi_{lsj}(r, k)}{r}, \tag{1}$$

where the internal wave function of the α-d system is $\chi_{I\mu s\sigma}$, with $I = 0$ and $s = 1$. $\varphi_{lsj}(r, k)$ describes the α-d relative radial motion with asymptotic wave-number k, orbital angular momentum l and total angular momentum j.

The radial continuum states $\varphi_{lsj}(r, k)$ in Eq. (1) are not square-integrable. However, Ref. [9] provides a prescription for constructing square-integrable wave functions known as bin states. A bin state $u^{(i)}_\beta(r)$ is obtained by a superposition of scattering wave functions within a given interval i, of continuum k values, $k_{i-1} < k < k_i$, *i.e.*,

$$u^{(i)}_{\beta=lsj}(r) = \sqrt{\frac{2}{\pi\eta_l}} \int_{k_{i-1}}^{k_i} w_i(k, l) e^{-i\delta_k(l)} \varphi_{lsj}(r, k) dk, \tag{2}$$

where $\delta_k(l)$ are scattering phase-shifts of φ_β and $w_i(k, l)$ are weight functions defined by,

$$\eta_l = \int_{k_{i-1}}^{k_i} |w_i(k, l)|^2 \, dk. \tag{3}$$

Actually, the weight functions w_i associated to non-resonant bin states are usually set as $w_i(k, l) = 1$, while for resonant states $w_i(k, l) = sin[\delta_k(l)]$.

The total wave function of the three-body system (α-d-$target$) is given by,

$$\Psi(\mathbf{R}, \mathbf{r}, \xi) = \sum_q \sum_\beta F_{\beta q}(\mathbf{R}) \psi^P_\beta(\mathbf{r}) \otimes \Phi^T_q(\xi), \tag{4}$$

where $\Phi^T_q(\xi)$, $q = 0, 1, 2, 3..$ correspond to the ground and inelastic states of the target satisfying $H^T\Phi^T_q(\xi) = \varepsilon^T_q \Phi^T_q(\xi)$. $F_{\beta q}(\mathbf{R})$ represents the projectile-target relative motion in the βq-channel.

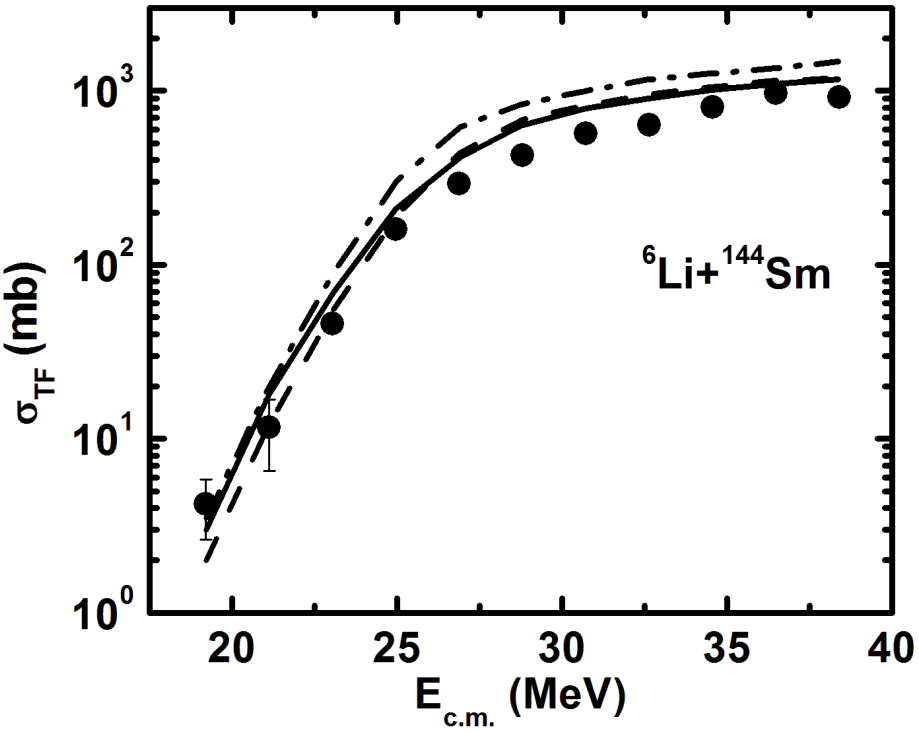

Figure 1. Total fusion cross section for ^{6}Li+^{144}Sm with the full breakup space of ^{6}Li (solid line), without excited states of the target (dashed line) and without breakup states of the projectile (dashed-dotted line).

Projecting the equation of motion of the system onto the projectile states β and onto the excited states of the target q, the following coupled equations are obtained,

$$\left[\hat{T}_R + U^{(J)}_{\beta q,\beta q}(R) - (E - \varepsilon_\beta - \varepsilon^T_q)\right] F^{(J)}_{\beta q}(R) = -\sum_{\beta' q'} U^{(J)}_{\beta q,\beta' q'}(R) F^{(J)}_{\beta' q'}(R). \tag{5}$$

Here, ε_β is the excitation energy of the projectile in the β-state. $U^{(J)}_{\beta q,\beta q}$ and $U^{(J)}_{\beta q,\beta' q'}$ are the radial dependent diagonal and non-diagonal matrices of the interaction potentials $\hat{V}_{dT} + \hat{V}_{\alpha T}$, where $\hat{V}_{dT}$ and $\hat{V}_{\alpha T}$ are the nuclear interactions between the deuteron and α-particle with the target. Notice that $U^{(J)}_{00,00}$ corresponds to the elastic incident channel. As a matter of fact, the interaction potential matrices are given by,

$$U^{(J)}_{\beta q \beta' q'}(R) = < u_\beta \Phi^T_q \left| \hat{V}_{dT}(\mathbf{r}_{dT}, \xi) + \hat{V}_{\alpha T}(\mathbf{r}_{\alpha T}, \xi) \right| u_{\beta'} \Phi^T_{q'} >, \tag{6}$$

where $\mathbf{r}_{dT} = \mathbf{R} - \frac{2}{6}\mathbf{r}$ and $\mathbf{r}_{\alpha T} = \mathbf{R} + \frac{4}{6}\mathbf{r}$ represent the radial distance between the fragments and the target. The integrations in Eq.(6) are carried out over the internal radial coordinate $\mathbf{r}$, the angular coordinates of $\mathbf{R}$ and the internal coordinates of the target ξ.

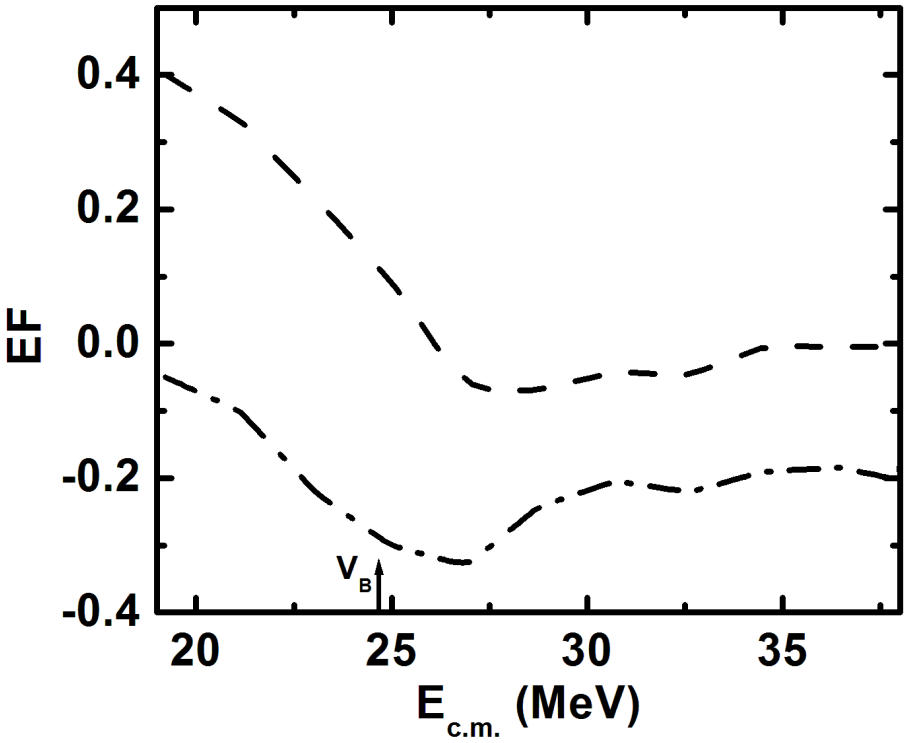

Figure 2. Fusion enhancement and suppression factors from excited states of ^{144}Sm (dashed line) and from breakup states of ^{6}Li (dashed-dotted line).

3. Calculations

3.1. Discretization of continuum space and interaction potentials

The ground state and discretized breakup states of $^{6}\text{Li}\rightarrow d+\alpha$ are constructed by using the interaction given in Ref.[38]. The discretization of the continuum is made as follows. The maximum angular momentum for the relative motion of the fragments is $l_{max}=3$, larger values do not have any effect on the calculated cross sections. So, bin states are constructed from an initial energy $\varepsilon_0=0$ MeV (above the threshold energy $E_{thres}=-1.47$ Mev) up to a maximum energy $\varepsilon_{\max}=6.8$ MeV. For states with $l=0$, $j^\pi=1^+$ and $l=1$, $j^\pi=0^-,1^-,2^-$ an energy step is fixed at $\Delta\varepsilon=0.5$ MeV. Finer and variable steps are used for resonant states $l=2$, $j^\pi=3^+,2^+$, 1^+, so as to obtain centroid excitation energies and widths close to the corresponding measured values [38]. For bin states $l=3$, $j^\pi=4^+,3^+,2^+$, a larger step $\Delta\varepsilon=1.0$ MeV is used. Convergence tests at $\varepsilon_{\max}=7.0, 7.5$ and 8.0 MeV were done with no effect on fusion. Similarly, larger steps $\Delta\varepsilon=0.75$ and 1.0 MeV were used with no appreciable effect. Coulomb and nuclear potential multipoles are included up to $L_Q=4$.

As for the nuclear interactions between the fragments α and d and the target of Eq.(6), we use the same potentials as in our previous work for elastic scattering of ^{6}Li+^{144}Sm [41]. That is, the systematic Woods-Saxon potential of Ref. [42] for $\hat{V}_{dT}$ and the density dependent double-folding Sao Paulo potential (SPP) for the $\hat{V}_{\alpha T}$ [43, 44]. These potentials have been modified to account for vibrational and deformed effects of the excited states of the target. In the calculations, the following excited states are included. For the spherical ^{144}Sm, the 2^+ (1160 keV) and 3^- (1810 keV) with $\beta_2=0.087$ and $\beta_3=0.15$, while for the deformed ^{154}Sm, the 2^+ (82 keV) and 4^+

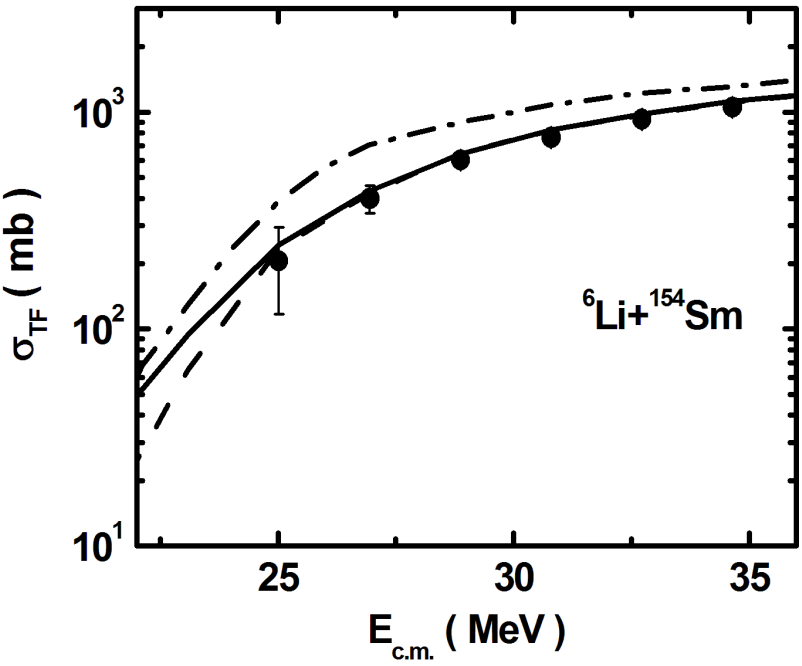

Figure 3. The same as Fig.1 but for ^{154}Sm.

(267 keV) states, with deformation parameters $\beta_2 = 0.34$ and $\beta_4 = 0.08$ [45, 46, 47].

It is important to point out that, the inelastic excitations of the target might be very important, specially in the case of the interaction with the strongly deformed ^{154}Sm target. Because of the limitations of the computational code that will be used to account for the collective degrees of freedom of the targets, we adopted the following approximations. First, we considered that the inelastic and breakup processes of the projectile can not occur at the same time. Then, to calculate the coupling matrix elements $U^J_{\beta=0,\beta'=0}(R)$, the single folding of the sum of the interaction potentials over the projectile g.s. wave function ($< u_0|\hat{V}_{dT}+\hat{V}_{\alpha T}|u_0 >$) is calculated and expanded in multipoles, as in the usual coupled channel calculations.

3.2. Total fusion and effect of resonance and non-resonance states of ^6Li

CDCC calculations of fusion between the ^{6}Li projectile with targets ^{144}Sm and ^{154}Sm for incident energies around and above the Coulomb barriers, are performed with the code FRESCO [48]. To calculate total fusion cross section σ_{TF}, two short range imaginary Woods-Saxon potentials $W_{\alpha-T}$ and W_{d-T} are considered to account for absorption of the α-particle and *deuteron* by the target. $W_{\alpha-T}$ depends on the radial distance between the α-particle and the target, while W_{d-T} on the radial distance between the *deuteron* and the target. The parameters of these potentials are fixed with strength $W = 25$ MeV, reduced radius $r = 0.9$ fm and diffuseness $a = 0.1$ fm for both ^{144}Sm and ^{154}Sm. Absorption by these potentials happens inside the corresponding Coulomb barriers $V_{B,d} = 13.92$ MeV, $R_{B,d} = 6.4$ fm and $V_{B,\alpha} = 26.5$ MeV, $R_{B,\alpha} = 6.83$ fm respectively. So, the incident flux that passes above or through the barrier, that is inside the short-range potential contributes to fusion. For the system ^{6}Li+^{144}Sm, Fig.1 shows the results for σ_{TF} (solid-line), the calculation without couplings from excited states of the target (dashed-line) and the calculation for the elastic channel, i.e., without couplings to continuum breakup states of the projectile or excited states of the target (dashed-dotted line). These results show

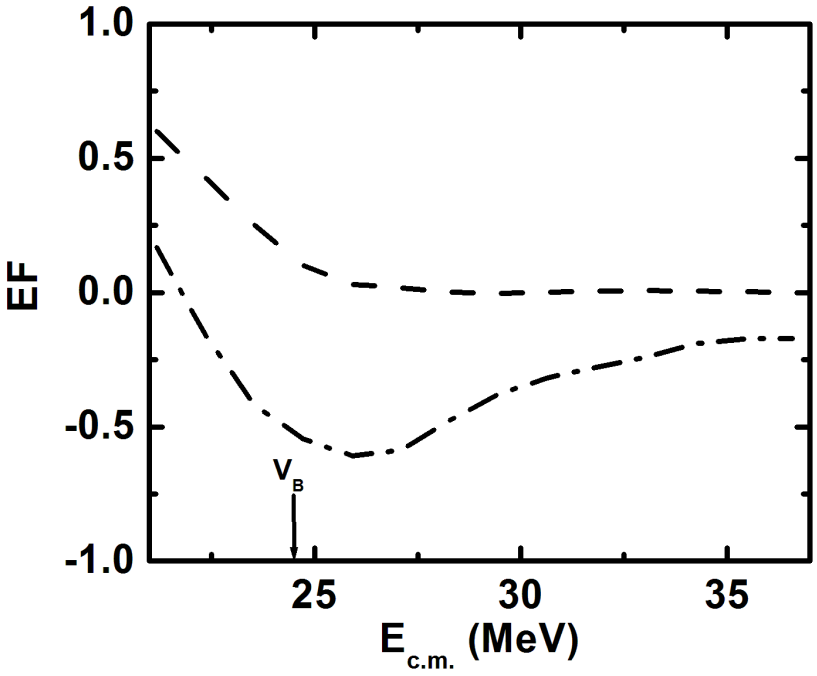

Figure 4. The same as Fig.2 but for ^{154}Sm.

that the calculated total fusion is above the data for energies above the barrier, however there is better agreement around and below the barrier. The total fusion data of Fig.1 are obtained by the sum of complete and incomplete fusion data of Refs. [28, 29]. Fig.2 shows the numerical effect EF on total fusion due to couplings from inelastic excited states of ^{144}Sm (dashed-line) and from continuum breakup states of ^{6}Li (dashed-dotted-line), where the EF is defined by,

$$EF = 1 - \frac{\sigma_{F,n}}{\sigma_{TF}}, \tag{7}$$

here, $n = 1, 2$ for inelastic and breakup couplings respectively. That is, $\sigma_{F,1}$ is the fusion cross section when the inelastic states of the target are omitted, and $\sigma_{F,2}$ when breakup states of the projectile and excited states of the target are not considered. It is observed that couplings to inelastic excited states of ^{144}Sm enhance fusion, particularly for energies below the Coulomb barrier. Here, the enhancement factor EF reaches a value of about 38% at $E_{c.m.} = 20$ MeV. On the other hand, the effect of couplings to breakup states of the projectile produces a net fusion suppression for all energies. The strength of the suppression factor EF increases as the collision energy decreases towards the barrier V_B then to then decrease at lower energies. That is, breakup state couplings produce a net repulsive potential that increases the fusion barrier and therefore reduces fusion. Figs.3 and 4 show the corresponding results for ^{154}Sm. The solid-line of Fig.3 presents the total fusion calculation, while the circles represent the data of Ref. [34]. The dashed-line of Fig. 4 shows that the effect of the excited states of the deformed ^{154}Sm is stronger than for the spherical ^{144}Sm at energies below the barrier. The enhancement factor EF reaches a value of about 50% at $E_{c.m.} = 22$ MeV, while for ^{144}Sm is about 30%. The dashed-dotted line of Fig. 3, shows that breakup state couplings of the projectile are essential to fit the data. This can be seen in Fig. 4, where is observed that these couplings produce a net repulsive effect that rises the barrier. On the other hand, breakup state couplings are more important for ^{154}Sm than for ^{144}Sm as shown by the dotted-dashed lines of Figs. 2 and 4.

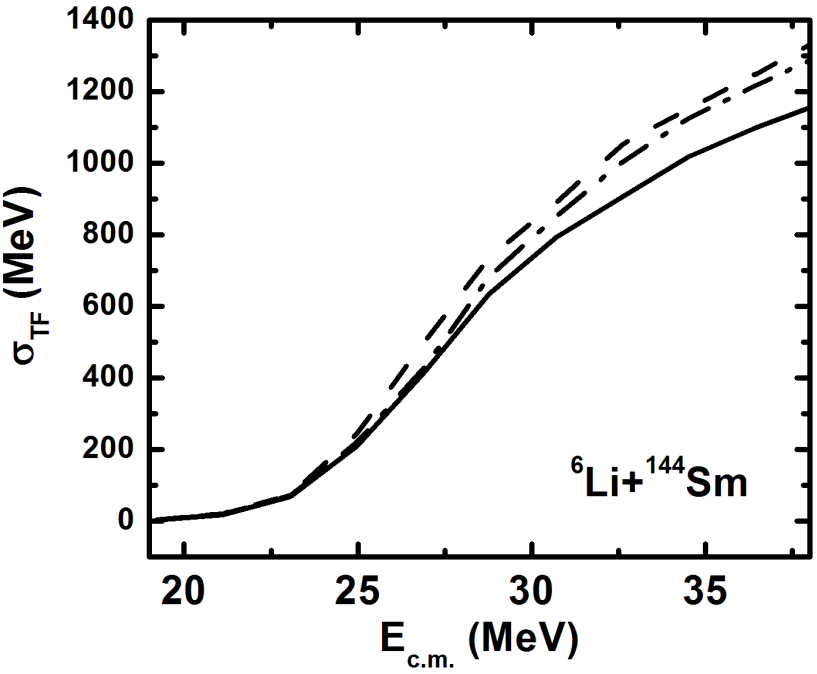

Figure 5. Effect of resonance breakup states of ^{6}Li on total fusion with ^{144}Sm target. The solid-line represents the calculation with the full discretized breakup space. The dashed-line shows the calculation with couplings among resonance states of ^{6}Li, while the dashed-dotted line for couplings among non-resonance states.

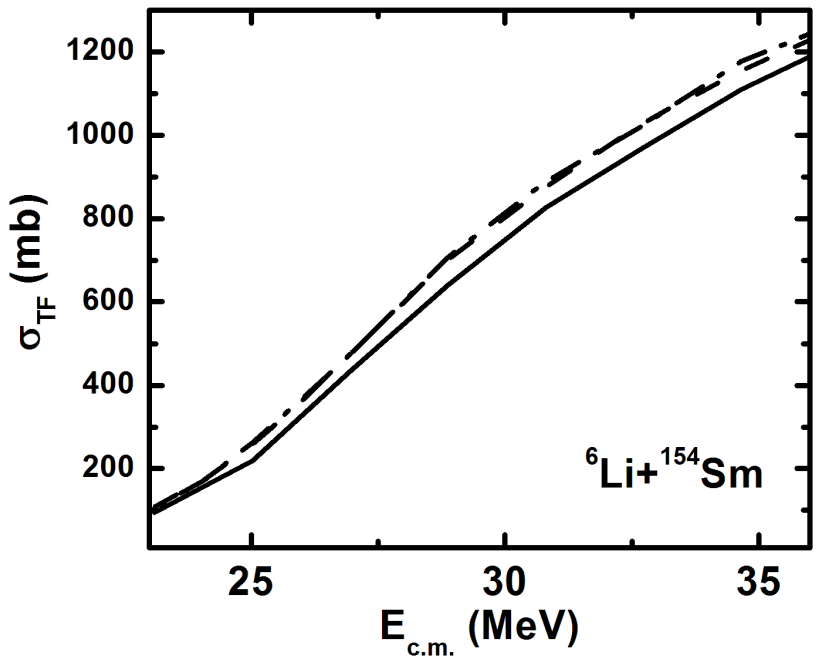

Figure 6. The same as Fig.5 but for ^{154}Sm.

Next, we present the calculations of the effect on total fusion from resonance breakup states $l = 2$, $j^{\pi} = 3^{+}, 2^{+}$, 1^{+} of the weakly bound nucleus ^{6}Li. The procedure is the same at that used in Refs. [40, 41], where a study of the effect of these resonances on elastic scattering was presented. Two different calculations are performed, namely, fusion is calculated when resonance states are excluded from the full discretized energy space, then when only couplings between the elastic channel and resonance state couplings are considered. The results are shown in Fig.5 for ^{144}Sm and Fig.6 for ^{154}Sm. The solid-lines represent the calculation with the full discretized energy space, the dashed-lines corresponds to the case when only couplings between resonance states are included, and the dashed-dotted lines when resonance states are omitted from the full space. It is observed that, the effect of resonance couplings are more important for ^{144}Sm than for ^{154}Sm. Also, fusion cross section with resonance and non-resonance sub-spaces are higher than the calculation with the full discretized energy space for all the collision energies considered. This implies that the net polarization potentials that appear from separate couplings between resonance and non-resonance states are repulsive. These potentials suppress fusion at all energies. Besides, it is seen that the suppression increases as the collision energy increases, this is more evident for ^{144}Sm than for ^{154}Sm.

4. Summary and conclusions

CDCC calculations of total fusion cross sections have been presented for the nuclear systems ^{6}Li with targets ^{144}Sm and ^{154}Sm at energies around and above the Coulomb barrier. In the CDCC calculations, resonance and non-resonance states of ^{6}Li are discretized up to a maximum energy of 6.8 MeV and discretization steps such that centroid energies of the resonances and widths are close to the experimental values. To account for the effect of excited states of the targets on fusion, low-lying excited states are included in the calculations. The cluster structure of the projectile $^{6}\text{Li} \rightarrow \alpha + d$ is assumed, with global nuclear interactions for the α-*target* and *d-target* sub-systems. For all of the energies studied in this work, it has been shown that calculations with coupling to only the elastic channel are insufficient to fit the fusion data, so, couplings to breakup states of ^{6}Li are very important. On the other hand, the effect of inelastic states of the targets produce attractive polarizations, that in turn, lower the fusion barrier and hence increase fusion. This effect is larger for the deformed ^{154}Sm than for the spherical ^{144}Sm. Short-range imaginary fusion potentials, inside the Coulomb barrier, have been used for the calculation of total fusion. So, complete and incomplete fusion are accounted for, when both fragments are absorbed or only one is captured. On the same footing, the effect on total fusion due to couplings from resonance state couplings of ^{6}Li, namely, $l = 2$, $J^{\pi} = 3^{+}, 2^{+}$ and 1^{+} has been calculated. This effect has been calculated by following two approaches, (a) by omitting the states corresponding to the resonances from the whole energy discrete space and (b) by considering only resonance state couplings. The effects of resonance and non-resonance couplings are stronger for ^{144}Sm than for ^{154}Sm. This is due to the nuclear potentials used for the interactions between the fragments α and d with ^{144}Sm, which are less attractive than those for ^{154}Sm. So, since the Coulomb interaction is the same for both targets, the effect of repulsive couplings from resonance and non-resonance states is more apparent for ^{144}Sm than for ^{154}Sm.

Acknowledgments

Financial support: A. Gómez Camacho from CONACYT, México.

References

[1] L.F. Canto, P.R.S. Gomes, R. Donangelo, M.S. Hussein, Phys. Rep., **424**, 1 (2006).
[2] J.F. Liang, C. Signorini, Int. J. Mod. Phys. E **14**, 1121 (2005).
[3] N. Keeley, R. Raabe, N. Alamanos, J.L. Sida, Prog. Part. Nucl. Sci. **59**, 579 (2007).
[4] L.F. Canto, P.R.S. Gomes, R. Donangelo, J. Lubian M.S. Hussein, Phys. Rep., **596**, 1 (2015).

[5] P.R.S. Gomes *et al.*, *few-body Systems* **57**, 165 (2016).
[6] M. Dasgupta *et al.*, Phys. Rev. Lett. **82**, 1395 (1999), Phys. Rev. C **66**, 04602(R) (2002), Phys. Rev. C **70**, 024606 (2004).
[7] C. Signorini *et al.*, Eur. Phys. J. A **5**, 7 (1999).
[8] P.R.S. Gomes, *et al.*, Phys. Lett. **B634**, 356 (2006), Phys. Rev. C **73**, 064606 (2006).
[9] Y. Sakuragi, M. Yahiro, M. Kamimura, Prog. Theor. Phys. Suppl. **89**, 1 (1986).
[10] Y. Sakuragi, M. Yahiro, M. Kamimura, Prog. Theor. Phys. **70**, 1047 (1983).
[11] N. Austern, Y. Iseri, M. Kamimura, M. Kawai, G. Rawitscher, M. Yahiro, Phys. Rep. **154**, 125 (1987).
[12] C. Beck , N. Keeley , A. Diaz-Torres, Phys. Rev. C **75**, 054605 (2007).
[13] J.P. Fernandez-Garcia, *et al.*, Phys. Lett. B **693**, 310 (2010).
[14] K. Zerva *et al.*, Phys. Rev. C **80**, 017601 (2009).
[15] K. Rusek, N. Keeley, A. Pakou, A. Alamanos, Nucl. Phys. A **784**, 13 (2007).
[16] N. Keeley, R.S. Mackintosh, C. Beck, Nucl. Phys. A **380**, 1 (2010).
[17] N. Keeley, K. Rusek, Phys. Lett. B, **375** (1996).
[18] D.R. Otomar, J. Lubian, P.R.S. Gomes, Eur. Phys. J. A. **46**, 285 (2010).
[19] G.R. Keeley *et al.*, Phys. Rev. C **63**, 024601 (2000).
[20] A. Pakou, *et al.*, Phys. Rev. C **69**, 054602 (2004).
[21] A. Pakou, *et al.*, Eur. Phys. J A **39**, 187 (2009).
[22] D.R. Otomar, *et al.* Phys. Rev. C **80** 034614 (2009).
[23] L.F. Canto, J. Lubian, P.R.S. Gomes, M.S. Hussein, Phys. Rev. C **80** 047601 (2009).
[24] J. Lubian, T. Correa, E.F. Aguilera, L.F. Canto, A. Gomez Camacho, E.M. Quiroz, P.R.S. Gomes, Phys. Rev. C **79**, 064605 (2009).
[25] B. Paes, J. Lubian, P.R.S. Gomes, V. Guimaraes, Nucl. Phys. A **890**, 1 (2012).
[26] J. Rangel, J. Lubian, L.F. Canto, P.R.S. Gomes, Phys. Rev. C **93**, 054610 (2016).
[27] S.P. Hu, *et al.*, Phys. Rev. C **91**, 044619 (2015).
[28] P.K. Rath, S. Santra, N.L. Singh, R. Tripathi, V.V. Parkar, B.K. Nayak, K. Mahata, R. Palit, Suresh Kumar, S. Mukherjee, S. Appannababu, R.K. Choudhury, Phys. Rev. C **79**, 051601 (2009).
[29] P.K. Rath, *et al.*, Nucl. Phys. A **874**, 14 (2012).
[30] N.T. Zhang, *et al.*, Phys. Rev. C **90**, 024621 (2014). 1121 (2005).
[31] Y.D. Fang, *et al.*, Phys. Rev. C. **91**, 014608 (2015).
[32] Bing Wang, Wei-Juan Zhao, P.R.S. Gomes, En-Guang Zhao, Shan-Gui Zhou, Phys. Rev. C **90**, 034612 (2014).
[33] Bing Wang, Wei-Juan Zhao, A. Diaz-Torres, En-Guang Zhao, Shan-Gui Zhou, Phys. Rev. C **93**, 014615 (2016).
[34] M.F. Guo, G.L. Zhang, P.R.S. Gomes, J. Lubian, E. Ferioli, Phys. Rev. C **94**, 044605 (2016).
[35] L.F. Canto, P.R.S. Gomes, J. Lubian, L.C. Chamon, E. Crema, Nucl. Phys. A. **821**, 51 (2009).
[36] L.F. Canto, P.R.S. Gomes, J. Lubian, L.C. Chamon, E, Crema, J. Phys. G. **36**, 015109 (2009).
[37] P.R.S. Gomes, J. Lubian, L.F. Canto, Phys. Rev. C. **79**, 027606 (2009).
[38] A. Diaz-Torres, I.J. Thompson and C. Beck, Phys. Rev. C **68**, 044607 (2013).
[39] A. Diaz-Torres and I.J. Thompson, Phys. Rev. C **65**, 024606 (2002).
[40] A. Gómez Camacho, A. Diaz-Torres, P.R.S. Gomes and J. Lubian, Phys. Rev. C **91**, 014607 (2015).
[41] A. Gómez Camacho, A. Diaz-Torres, P.R.S. Gomes and J. Lubian, Phys. Rev. C **93**, 024604 (2016).
[42] H. An and C. Cai, Phys. Rev. C **73**, 054605 (2006).
[43] L.C. Chamon *et al.*, Phys. Rev. Lett. **79**, 5218 (1997).
[44] L.C. Chamon *et al.*, Phys. Rev. C **66**, 014610 (2002).
[45] S. Raman, C.W. Nestor Jr, P. Tikkanem, At. Data Nucl. Data Tables **78**, 1 (2001).
[46] T. Kibedi, R.H. Spear, At. DataNucl. Data Tables **80**, 35 (2001).
[47] J.R. Leigh *et al.*, Phys. Rev. C **52**, 3151 (1995).
[48] I.J. Thompson, Comput. Phys. Rep. **7,** 167 (1988).